Probing quantum phase transitions via quantum speed limits

M. Suman,* S. Aravinda,† and Ranjan Modak‡
Department of Physics, Indian Institute of Technology Tirupati, Tirupati 517619, India

(Received 26 January 2024; revised 23 May 2024; accepted 8 July 2024; published 31 July 2024)

The quantum speed limit (QSL) is the lower bound on the time required for a state to evolve to a desired final state under a given Hamiltonian evolution. Three well-known QSLs exist: the Mandelstam-Tamm (MT), Margolus-Levitin (ML), and dual ML (ML*) bounds. We consider one-dimensional systems that undergo a delocalization-localization transition in the presence of quasiperiodic and linear potential. By performing sudden quenches across the phase boundary, we find that the exact dynamics gets captured very well by QSLs. We show that the MT bound is always tighter in the short-time limit for any arbitrary state, while the optimal bound for the time of orthogonalization (time required to reach the orthogonal state) depends on the choice of the initial state. Further, for extreme quenches, we prove that the MT bound remains tighter for the time of orthogonalization and it can qualitatively describe the nonanalyticity in free energy for the dynamical quantum phase transition. We also demonstrate that the localization-delocalization transition point can be exactly identified from QSLs for two of the models of noninteracting fermions. Further, we also show that even for interacting systems, an ergodic to many-body localization transition can also be efficiently predicted from QSLs, whose computation cost is much less than other diagnostic tools.

DOI: 10.1103/PhysRevA.110.012466

I. INTRODUCTION

The quantum speed limit (QSL) is a fundamental limit in quantum mechanics on the rate at which any quantum system evolves under a dynamical process [1–4]. It essentially provides a bound on the minimal time required to transport a system from its initial state to a final state under unitary evolution. Apart from this theoretical interest in understanding the basic features of a quantum system, the quantum speed limit also remains an integral part of recent advances in quantum engineering to investigate how quickly a transition can take place between distinguishable states [5,6]. In other practical examples, such as to estimate the speed of quantum simulations involving quantum information processing [7], quantum computation, and quantum metrology [8–10]; identifying decoherence time [8,11,12]; experimentally measuring the environment-assisted speedup [13]; and even in the context of the machine learning [14], the QSL plays a vital role.

The first QSL was proposed by Mandelstam and Tamm (MT), who realized that fundamentally the time-energy uncertainty relation corresponds to the intrinsic timescale of unitary evolution in quantum mechanics [2]. This relation restricts the minimal time τ_{MT} for a unitary system to propagate between two states that depend on its energy spread. On the other hand, the time limit τ_{ML} was derived by Margolus and Levitin (ML) [15], which depends on the mean energy measured relative to the energy of the the ground state. Very recently, a QSL was proposed which is referred to as the dual ML bound (ML*) [16]. This bound is essentially equivalent to the ML bound in time-reversed dynamics. While Levitin and Toffoli unified the MT and ML bounds [17], with the addition of the ML* bound all three QSLs can be unified and the lower bound for the time required for arriving at an orthogonal state (time of orthogonalization) $t_\perp$ can be written as

$$t_\perp \geqslant \tau_{\mathrm{QSL}} = \max\{\tau_{\mathrm{MT}}, \tau_{\mathrm{ML}}, \tau_{\mathrm{ML}^*}\}. \tag{1}$$

The phase transition in many-body systems is a most illustrious phenomenon. In equilibrium many-body systems, it is witnessed as the nonanalytical behavior of its partition function at the thermodynamic limit [18,19]. Motivated by this, the dynamical quantum phase transition (DQPT) is proposed as nonanalytical behavior in the time expansion of the overlap amplitude of the time-evolved initial quantum state [20–23]. The DQPT is characterized by the occurrence of zeros in the Loschmidt echo $\mathcal{L}$ at specific critical times t_n^* [20,24,25], with the Loschmidt echo defined by $\mathcal{L}(t) = |\langle\psi_i|e^{-iH_f t}|\psi_i\rangle|^2$, where $|\psi_i\rangle$ is the ground state of the prequench Hamiltonian H_i and H_f is the postquench Hamiltonian. These zeros of $\mathcal{L}$ correspond to the nonanalytic behaviors of the dynamical free energy $f(t) = -\frac{1}{N}\ln\mathcal{L}(t)$ at those critical times [26]. In general, exact zeros of $\mathcal{L}$ or nonanalyticities of the dynamical free energy only occur as the system size N approaches the thermodynamic limit; however, recent studies have shown that they can be observed for finite systems as well [27,28]. The critical time at which the first exact zeros of $\mathcal{L}$ occurs, i.e., t_1^*, can be identified as the minimum time required for an initial state to reach an orthogonal state under the time evolution. From the definition, it is obvious that $t_1^* \geqslant \tau_{\mathrm{QSL}}$.

The DQPT has been mostly observed in systems that go through an underlying equilibrium phase transition and it is a

*Contact author: msuman.physics@gmail.com
†Contact author: aravinda@iittp.ac.in
‡Contact author: ranjan@iittp.ac.in

 ©2024 American Physical Society

generic feature of quantum quenches across quantum critical points. It also has been observed in topological [29,30] and Floquet systems [31,32]. The DQPT has also been realized in experiments [33,34].

Our main goal here is to investigate the QSL for a Hamiltonian system that can be probed in experiments, e.g. in cold-atom experiments. Given that the systems that show the signature of the DQPT have the unique feature of having zeros in the time evolution of $\mathcal{L}$, they become a natural choice to study QSLs for the time of orthogonalization. In this work we focus on systems that display the DQPT while quenching across the localization-delocalization transition point [35–37]. The dynamical regimes of applicability of particular QSLs have been studied for few-level systems (qutrits) [16], and it is important to investigate them in experimentally realizable physical many-level systems.

The aim of our study is twofold: (i) to investigate which one of the QSLs can more efficiently capture short-time dynamics and the nonanalytic nature of the dynamical free energy and (ii) to determine if the localization-delocalization transition point can be identified using QSLs instead of studying the exact dynamics of the system. We attempt to answer these questions by studying two one-dimensional noninteracting models, specifically, the Aubry-Andre (AA) model [38] and the Wannier-Stark model, which supports the localization transition [39,40], and the one-dimensional interacting many-body Hamiltonian, which shows the transition from the ergodic phase to the many-body localized (MBL) phase [41].

The paper is organized as follows. In Sec. II we discuss the preliminaries, which includes models we study in this work and also different QSLs. Analytical results for extreme quenches are presented in Sec. III, followed by numerical results in Sec. IV. We summarize in Sec. V.

II. PRELIMINARIES

Here we briefly discuss the models investigated in this paper and also define the different QSLs we use extensively to compare with exact dynamics in the subsequent sections.

A. Model

We study a system that is described by the Hamiltonian on a one-dimensional lattice,

$$H(J,\Delta) = -J\sum_{j=1}^{N}(c_{j+1}^{\dagger}c_j + \text{H.c.}) + \Delta\sum_{j=1}^{N}\epsilon_j n_j, \quad (2)$$

where c_j and $c_j^{\dagger}$ are the fermionic annihilation and creation operators, respectively, $n_j = c_j^{\dagger}c_j$ is the number operator. J is the hopping strength, and Δ is the strength of the on-site potential, in units of $\hbar$. We consider two types of on-site potentials: an incommensurate potential $\epsilon_n = \cos(2\pi\alpha n)$, with α an irrational number, and a linear potential $\epsilon_n = n$. The former is known as the AA model and shows a localization transition at $\Delta = 2J$ [38]. In the case of the latter, any infinitesimal value of Δ is sufficient to localize all the states, a phenomenon known as Wannier-Stark localization [39,40]. Both of these Hamiltonians have been realized in experiments [42–48]. Motivated by the experimental setup, we mostly focus on a quench from the localized phase to the delocalized phase. Initially, we prepare our system as an eigenstate $|\psi_0\rangle$ of $H(\Delta_i)$, with Δ_i very large and keeping J constant throughout the process. Next we quench the system to the delocalized phase and study the time evolution of the Loschmidt echo $\mathcal{L}(t)$. Later in the paper we investigate the quench from the delocalized phase to the localized phase as well. For all our numerical results presented in the paper, we choose $\alpha = (\sqrt{5}-1)/2$, open boundary conditions, and $J = 1$.

We also test our prediction for the interacting many-body systems of the fermions, and the Hamiltonian is given by [49]

$$H_{\text{MBL}}(J,\Delta,V) = -J\sum_{j=1}^{N}(c_{j+1}^{\dagger}c_j + \text{H.c.}) + \Delta\sum_{j=1}^{N}\epsilon_j n_j + V\sum_{j=1}^{N} n_j n_{j+1}, \quad (3)$$

where V is the nearest-neighbor interaction strength between the fermions, in units of $\hbar$. In the absence of the on-site potential, i.e., $\Delta = 0$, the Hamiltonian is integrable and the model is solvable within the Bethe-ansatz framework [50]. However, for nonzero Δ, there are no analytical solutions for this Hamiltonian, forcing us to use only numerical methodology. In our analysis we focus on the quasirandom on-site potential $\epsilon_j = \cos(2\pi\alpha j + \phi)$ with some phase factor ϕ. This Hamiltonian shows an ergodic to many-body localization phase transition [41] as the strength of the on-site potential increases.

B. Quantum speed limits

Three QSLs bounds have already been introduced in the Introduction, where the consideration was that the time-evolved state is orthogonal to the initial state $|\psi_0\rangle$. After a sudden quench is performed using a postquench Hamiltonian $H(\Delta_f)$, QSLs can be derived for any arbitrary state that is not necessarily orthogonal to $|\psi_0\rangle$. Three QSL bounds for any time-evolved state $|\psi_T\rangle$ are given by

$$\begin{aligned} T_{\text{MT}} &= \frac{1}{\Delta H}\arccos(|\langle\psi_0|\psi_T\rangle|), \\ T_{\text{ML}} &= \frac{2}{\pi(\langle H\rangle - E_0)}[\arccos(|\langle\psi_0|\psi_T\rangle|)]^2, \\ T_{\text{ML}^*} &= \frac{2}{\pi(E_{\max} - \langle H\rangle)}[\arccos(|\langle\psi_0|\psi_T\rangle|)]^2. \end{aligned} \quad (4)$$

The average $\langle H(\Delta_f)\rangle$ and uncertainty $\Delta H = \sqrt{\langle H^2(\Delta_f)\rangle - \langle H(\Delta_f)\rangle^2}$ are computed with respect to the initial state. Here E_0 and $E_{\max}$ are the ground state and the highest excited state energy of the postquench Hamiltonian $H(\Delta_f)$. In the subsequent sections, we compare the results obtained using the exact dynamics and different QSLs, using the above expressions extensively.

III. ANALYTICAL RESULTS FOR EXTREME QUENCHES

For a general quench $\Delta_i \to \Delta_f$ across the phase boundary, computing QSLs analytically is not that straightforward.

However, for extreme quenches, i.e., $\Delta_i \to 0$ to $\Delta_f \to \infty$ (delocalized to localized) or $\Delta_i \to \infty$ to $\Delta_f \to 0$ (localized to delocalized), QSLs can be obtained analytically. Since we are quenching across the phase boundary, the final state is expected to be orthogonal to the initial state for the AA and Wannier-Stark models [35,37]. In this section we focus on such cases and demonstrate that the MT bound is always tighter for extreme quenches; it can also show a clear signature of the dynamical quantum phase transition.

Consider the Hamiltonian $H(J, \Delta = 0)$, which is exactly solvable, with the eigenstate and eigenenergy given by

$$|k\rangle = \frac{1}{N}\sum_{n=1}^{N} e^{ikn} c_n^\dagger |0\rangle, \quad E_k = 2J\cos(ka), \tag{5}$$

where $k = \frac{2\pi(l-N/2)}{aN} \in (-\frac{\pi}{a}, \frac{\pi}{a}]$ $(l = 1, \ldots, N)$ lies in the first Brillouin zone. These eigenstates are delocalized plane waves. Similarly, the Hamiltonian $H(J, \Delta \to \infty)$ has the eigenstate and eigenenergy

$$|m\rangle = \sum_{n=1}^{N} \delta_{nm} c_n^\dagger |0\rangle, \quad E_m = \Delta\epsilon_m, \tag{6}$$

respectively. These states are localized. Throughout this paper we refer to $|k\rangle$ as a delocalized state and $|m\rangle$ as a localized state in an extreme quench regime. Also, for analytical calculations we keep J constant, without mentioning it in the further calculation.

A. Quench from the localized phase to the delocalized phase

1. The AA model

First, we focus on the AA model and consider the case where the initial state is an eigenstate of the Hamiltonian $H(\Delta_i \to \infty)$, hence localized by definition. This state is quenched by the Hamiltonian $H(\Delta_f = 0)$. We set J to be constant throughout the quench. We study which bound is tighter for such a quench for the time of orthogonalization and also compare the QSL bound with the results obtained from the exact dynamics. To calculate the ML and MT bounds, we begin by calculating the expectation of the postquench Hamiltonian with respect to the initial state

$$\langle H(\Delta_f = 0)\rangle = \langle 0|c_m H c_m^\dagger|0\rangle = 0. \tag{7}$$

The expectation value is zero because diagonal elements of the Hamiltonian are zero. Similarly, the expectation value of the square of the Hamiltonian reads

$$\langle H^2(\Delta_f = 0)\rangle = 2J^2. \tag{8}$$

The details of the calculations are included in Appendix A. The above results are true for all m except $m = 1$ and $m = N$. Hence, the uncertainty in energy of the postquench Hamiltonian $\Delta H = \sqrt{\langle H^2\rangle - \langle H\rangle^2} = \sqrt{2}J$. By knowing the ground-state energy $E_0 = -2J$ of the quench Hamiltonian, the ML and MT bounds for the time of orthogonalization can be written as

$$\tau_{\mathrm{ML}}^{\infty\to 0} = \frac{\pi}{2(\langle H\rangle - E_0)} = \frac{\pi}{4J},$$
$$\tau_{\mathrm{MT}}^{\infty\to 0} = \frac{\pi}{2\Delta H} = \frac{\pi}{2\sqrt{2}J}, \tag{9}$$

from which it is obvious that $\tau_{\mathrm{MT}} > \tau_{\mathrm{ML}}$. Hence, for an extreme quench, the MT bound is always tighter than the ML bound.

Next, to understand whether τ_{MT} is a good approximation to the orthogonalization time $t_\perp$, we turn our attention towards deriving the results for the exact time evolution of the Loschmidt amplitude $\mathcal{G}(t)$, which reads [35]

$$\mathcal{G}(t) = \langle m|e^{-iH(\Delta_f)t}|m\rangle = \sum_{k=1}^{N}\langle m|^{-iH(\Delta_f)t}|k\rangle\langle k|m\rangle$$
$$= \sum_{k=1}^{N} e^{-2iJt\cos(ka)}|\langle m|k\rangle|^2 = \frac{1}{N}\sum_{k=1}^{N} e^{-2iJ\cos(ka)t},$$

where k is distributed from $-\pi/a$ to π/a. Hence, for a large system size $N \to \infty$, the summation can be replaced by an integration,

$$\mathcal{G}(t) = \frac{a}{2\pi}\int_{-\pi/a}^{\pi/a} e^{-2iJ\cos(ka)t}dk = \mathcal{J}_0(2Jt),$$

where $\mathcal{J}_0$ is the zeroth-order Bessel function, whose zeros occur at

$$t_\alpha^\star = \frac{x_\alpha}{2J}, \tag{10}$$

where x_α are roots of the Bessel function. From Eqs. (10) and (9) we find that the times of orthogonalization obtained from the QSL bound as well as from the exact dynamics are both independent of Δ_f. The exact first zero of $\mathcal{L}(t)$ occurs at $t_1^* = 1.2024/J \geqslant \tau_{\mathrm{MT}} = 1.1072/J$. Hence, the MT bound serves as a very good approximation for the exact result.

2. Wannier-Stark model

For the Wannier-Stark model, both the ML bound and the MT bound give the same result as that obtained for the AA model, as the eigenstates of the prequench Hamiltonian and the postquench Hamiltonian are the same for both models for extreme quenches. Also, the dual ML bound for the Wannier-Stark model is not defined, as this model does not have an upper spectral bound to its energy. The QSL bounds for the Wannier-Stark model are distinguished by a tilde:

$$\tilde{\tau}_{\mathrm{ML}}^{\infty\to 0} = \frac{\pi}{2(\langle H\rangle - E_0)} = \frac{\pi}{4J},$$
$$\tilde{\tau}_{\mathrm{MT}}^{\infty\to 0} = \frac{\pi}{2\Delta H} = \frac{\pi}{2\sqrt{2}J}. \tag{11}$$

The orthogonalization time obtained from the exact dynamics is also the same as before, i.e., $t_\alpha^* = x_\alpha/2J$.

B. Quench from the delocalized phase to the localized phase

1. The AA model

Here we consider the initial state as the eigenstate of the Hamiltonian $H(\Delta_i = 0)$ and the postquench Hamiltonian is the AA Hamiltonian $H(\Delta_f \to \infty)$. We compute $\langle k|H|k\rangle$ and $\langle k|H^2|k\rangle$ for the postquench Hamiltonian $H(\Delta_f \to \infty)$. In

the limit $N \to \infty$, they are given by

$$\langle H(\Delta_f \to \infty)\rangle = \frac{1}{N}\sum_{n,p=1}^{N} e^{-ink}\langle 0|c_n H c_p^\dagger|0\rangle e^{ipk}$$
$$= \frac{\Delta_f}{N}\sum_{n=1}^{N}\cos(2\pi\alpha n) \approx 0 \tag{12}$$

and

$$\langle H^2(\Delta_f \to \infty)\rangle = \frac{\Delta_f^2}{N}\sum_{n=1}^{N}\cos^2(2\pi\alpha n) \approx \frac{\Delta_f^2}{2}. \tag{13}$$

The energy uncertainty $\Delta H = \Delta_f/\sqrt{2}$ and the ground-state energy of the postquench Hamiltonian is $E_0 = -\Delta_f$. The QSL bound for the time of orthogonalization can be written as

$$\tau_{\rm ML}^{0\to\infty} = \frac{\pi}{2\Delta_f},$$
$$\tau_{\rm MT}^{0\to\infty} = \frac{\sqrt{2}\pi}{2\Delta_f}, \tag{14}$$

which automatically implies that $\tau_{\rm MT} > \tau_{\rm ML}$. Once again, to find out how tight the QSL bound is in comparison to the exact dynamics, we turn our attention to the exact results, and the time evolution of the exact Loschmidt amplitude can be written as [35]

$$\mathcal{G}(t) = \langle k|e^{-iH(\Delta_f)t}|k\rangle = \sum_{m=1}^{N}\langle k|e^{-iH(\Delta_f)t}|m\rangle\langle m|k\rangle$$
$$= \sum_{m=1}^{N} e^{-i\Delta_f\cos(2\pi\alpha m)t}|\langle m|k\rangle|^2.$$

Now from Eqs. (5) and (6), $|\langle m|k\rangle|^2 = 1/N$. Hence,

$$\mathcal{G}(t) = \frac{1}{N}\sum_{m=1}^{N} e^{-i\Delta_f\cos(2\pi\alpha m)t}.$$

For an irrational number α, the phase $2\pi\alpha m$ is distributed between $-\pi$ and π. In the $N \to \infty$ limit, the summation can be converted into an integral and

$$\mathcal{G}(t) \approx \frac{1}{2\pi}\int_{-\pi}^{\pi} e^{-i\Delta_f\cos(\theta)t}d\theta = \mathcal{J}_0(\Delta_f t).$$

The zeros of the Bessel function $\mathcal{J}_0(\Delta_f t)$ correspond to the zeros of the Loschmidt amplitude, which are given by

$$t_\alpha^* = \frac{x_\alpha}{\Delta_f}. \tag{15}$$

The first zero is $t_1^* = 2.4048/\Delta_f > \tau_{\rm MT} = 2.2214/\Delta_f$, and interestingly both the exact result and the MT bound are inversely proportional to Δ_f and they are reasonably close to each other.

2. Wannier-Stark model

Unlike the previous scenario, QSL bounds for the extreme quench from the delocalized phase to the localized phase give rise to different results for the Wannier-Stark model compared to the AA model. For the Wannier-Stark model, $\langle H(\Delta_f \to \infty)\rangle$ and $\langle H^2(\Delta_f \to \infty)\rangle$ are given by

$$\langle H(\Delta_f \to \infty)\rangle = \frac{1}{N}\sum_{n,p=1}^{N} e^{-ink}\langle 0|c_n H c_p^\dagger|0\rangle e^{ipk}$$
$$= \frac{\Delta_f}{N}\sum_{n=1}^{N} n = \Delta_f\frac{(N+1)}{2},$$
$$\langle H^2(\Delta_f \to \infty)\rangle = \frac{\Delta_f^2}{N}\sum_{n=1}^{N} n^2 = \Delta_f^2\frac{(N+1)(2N+1)}{6}. \tag{16}$$

The uncertainty $\Delta H = \Delta_f\sqrt{\frac{N^2-1}{2}}$. Noting that the ground-state energy of $H(\Delta_f \to \infty)$ is zero, the QSL bound can be written as

$$\tilde{\tau}_{\rm ML}^{0\to\infty} = \frac{\pi}{\Delta_f(N+1)},$$
$$\tilde{\tau}_{\rm MT}^{0\to\infty} = \frac{\sqrt{3}\pi}{\Delta_f\sqrt{N^2-1}}. \tag{17}$$

Once again, it is obvious that $\tilde{\tau}_{\rm MT} > \tilde{\tau}_{\rm ML}$, which automatically makes MT a tighter bound. Now to compare $\tilde{\tau}_{\rm MT}$ with the zeros of the exact Loschmidt amplitude, we compute $\mathcal{G}(t)$, i.e.,

$$\mathcal{G}(t) = \langle k|e^{-iH(\Delta_f)t}|k\rangle = \sum_{m=1}^{N}\langle k|e^{-iH(\Delta_f)t}|m\rangle\langle m|k\rangle$$
$$= \sum_{m=1}^{N} e^{-i\Delta_f mt}|\langle m|k\rangle|^2 = \frac{1}{N}\sum_{m=1}^{N} e^{-im\Delta_f t}.$$

With some simplifications, we can end up with $\mathcal{L}(t) = |\sin(x)/x|^2$, where $x = \Delta_f tN/2$. The $\mathcal{L}(t)$ has zeros at $t_n^* = \frac{2\pi n}{\Delta_f N}$. Hence, for a large but finite value of N, the first zero is given by $t_1^* = \frac{2\pi}{\Delta_f N} > \tilde{\tau}_{\rm MT}$. The important thing to note here is that the orthogonalization time is inversely proportional to the system size N, whereas for the AA model, the orthogonalization time was independent of N. In the thermodynamic limit $N \to \infty$, both $t_1^* \to 0$ and $\tilde{\tau}_{\rm MT} \to 0$.

C. Detection of the transition point

Our main finding from the preceding section was that, for the extreme quenches, $\tau_{\rm QSL} = \tau_{\rm MT}$, i.e., the MT bound is always tighter for the time of orthogonalization; we also obtained the exact expression for $\tau_{\rm MT}^{0\to\infty}$ and $\tau_{\rm MT}^{\infty\to 0}$. For the AA model, interestingly, it turns out that $\tau_{\rm MT}^{0\to\infty} = \tau_{\rm MT}^{\infty\to 0}$ when $\Delta_f = 2J$, which is also the transition point for this model.

If one were to draw a conclusion from the AA model that at the transition point $\tau_{\rm QSL}$ should be the same for two opposite extreme quenches, for the Wannier-Stark model, once again, one would expect that $\tilde{\tau}_{\rm MT}^{0\to\infty} = \tilde{\tau}_{\rm MT}^{\infty\to 0}$ at the boundary of the phase transition. This implies $\Delta_f = \sqrt{\frac{24}{N^2-1}}J$, and the transition point for the Wannier-Stark model should scale to zero as N^{-1} in the $N \to \infty$ limit. Indeed, it is well known that the transition point approaches zero for the Wannier-Stark model in the thermodynamic limit [37].

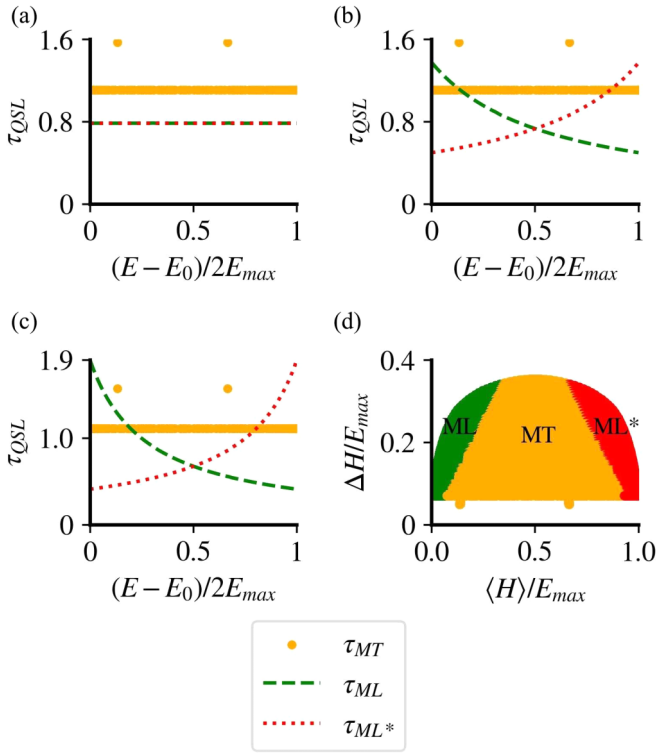

FIG. 1. Region of the best bounds. Each bound is plotted as a function of energy for (a) $\Delta_f = 0$, (b) $\Delta_f = 1$, and (c) $\Delta_f = 2$, with $\Delta_i = 1000$ and system size $N = 100$. (d) Plot of rescaled ΔH vs $\langle H\rangle$. The Hamiltonian's ground state is already set to zero $H = H(\Delta_i) - E_0$. The initial states are taken as eigenstates of $H(\Delta_i = 1000)$. The quench Hamiltonian $H(\Delta_f)$ is taken for different Δ_f, varying from 0 to 10.

IV. NUMERICAL RESULTS

Earlier, we focused on the extreme quenches. Here we show the numerical results for Δ_i and Δ_f, both of which are nonzero but finite. First, we discuss the quench from the localized phase to the delocalized phase. Then we show the results corresponding to the delocalized to localized quench. Finally, we demonstrate how the $\tau_{\rm QSL}$ can be used to detect the transition point for the AA and the Wannier-Stark Hamiltonian, along with the many-body Hamiltonian. Recall that for all numerical results we set $J = 1$.

A. Quench from the localized phase to the delocalized phase

We focus on the AA model and consider the situation where the initial state is still a highly localized eigenstate of $H(\Delta_i \gg 2)$, and $\Delta_f < 2$. It was shown in the preceding section that for $\Delta_f = 0$, the MT bound corresponding to the orthogonal time is tighter for any eigenstates of $H(\Delta_i \gg 2)$. From Fig. 1 it is clear that for $\Delta_f \neq 0$ the region of best bounds depends on the initial state, i.e., the energy eigenstate of $H(\Delta_i)$. Figures 1(b) and 1(c) show that for the high-energy and low-energy states, the ML* and ML bounds, respectively, are tighter, whereas for the intermediate-energy states the MT bound remains tighter. As expected, with decreasing Δ_f, more and more states start respecting the MT bound, and in the limit $\Delta_f \to 0$, the MT bound becomes tighter for all the states.

When this bound was derived, we excluded the state corresponding to the first and last lattice points. For the first and last lattice points the MT bound can be written as $\tau_{\rm MT} = \pi/2J$ (see Appendix A). Bounds at these points are always greater than the other points. Hence, in Fig. 1 we can see that those two points of the MT bound are always higher than the rest of the values. Note that this is simply the boundary effect, which will go away if we use periodic boundary conditions instead of open boundary conditions. The results shown in Fig. 1 can be well understood by investigating the energy expectation value and the uncertainty in energy for the postquench Hamiltonian. Figure 1(d) gives an idea about regimes in which the bound becomes tighter (note that we have subtracted the ground-state energy E_0 from the energy expectation $\langle H\rangle$). The states for which $\Delta H \geqslant \langle H\rangle$ correspond to the green-shaded ML-bound regime. Similarly, states with $\Delta H \geqslant E_{\rm max} - \langle H\rangle$ belong to the red shaded ML*-bound regime. The orange-shaded region corresponds to the MT bound. The upper limit of all these bounds is further constrained by Popoviciu's inequality [16,51], i.e.,

$$\Delta H \leqslant \sqrt{\langle H\rangle(E_{\rm max} - \langle H\rangle)}. \tag{18}$$

From this inequality, ΔH becomes maximum at $\langle H\rangle = E_{\rm max}/2$, that is, $\Delta H = E_{\rm max}/2$. At the intersection of the $\Delta H = \langle H\rangle$ and $\Delta H = E_{\rm max} - \langle H\rangle$ lines, all three bounds will coincide [16]. For our Hamiltonian H, the ΔH never saturates the Popoviciu's inequality. Hence all three bounds never coincide with each other.

While so far we have mostly focused on the bound corresponding to the time of orthogonalization $\tau_{\rm QSL}$, here we redirect our attention to a time window $[0, T]$, where $T < \tau_{\rm QSL}$. Figure 2 shows not only that the MT bound is tighter for the midspectrum states, but also that the differences between the exact dynamics and the bound are quite small. On the other hand, for low-energy states (and also for high-energy states) the bound is not that close to the exact result. Moreover, in Fig. 2(c) we study a particular case where the initial state and the postquench Hamiltonian are chosen in such a way that for some time the MT bound is tighter, followed by a crossover, and finally the ML bound becomes tighter.

The fact that in the initial time the MT bound is tighter can be well understood from Eq. (4) Inverting Eq. (4) the Loschmidt echoes corresponding to the bounds can be calculated as

$$\begin{aligned}\mathcal{L}(t_{\rm ML}) &= \cos^2\left(\sqrt{\frac{\pi\langle H\rangle t_{\rm ML}}{2}}\right),\\ \mathcal{L}(t_{\rm MT}) &= \cos^2(\Delta H t_{\rm MT}).\end{aligned} \tag{19}$$

At the crossover point both bounds are equal, i.e., $\Delta H T_{\rm cross} = \sqrt{\frac{\pi\langle H\rangle T_{\rm cross}}{2}}$; ($t_{\rm ML} = t_{\rm MT} = T_{\rm cross}$). Hence, we get the crossover time as

$$T_{\rm cross} = \frac{\pi\langle H\rangle}{2(\Delta H)^2}. \tag{20}$$

Also, the crossover takes place only if $\Delta H \geqslant \langle H\rangle$. Including this additional constrain, from Eq. (19) it can be seen that $\mathcal{L}(t_{\rm ML}) < \mathcal{L}(t_{\rm MT})\,\forall\, t < T_{\rm cross}$. This also can be observed in Fig. 2.

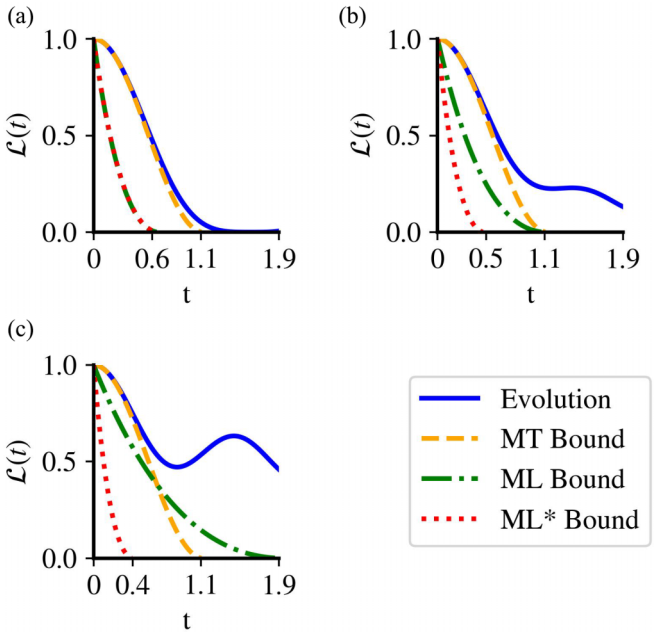

FIG. 2. State evolution of the system in different dynamical regimes, with energy equal to (a) -4.61, (b) -60.09, and (c) -100.00. From Eq. (4) the Loschmidt echo is plotted as a function of time as well as for exact state evolution. The initial Hamiltonian is taken to be $H(\Delta_i = 100)$ and the quench Hamiltonian is taken as $H(\Delta_f = 1.5)$. The system size is $N = 100$. (a) The MT bound dominates and the orthogonal time of the MT bound and the exact time evolution are quite close. (b) The time of orthogonalization of exact evolution is at $t_\perp = 5.4$. In this case the ML and MT bounds coincide. (c) The time of orthogonalization of exact evolution is $t_\perp = 33.9$. The ML bound dominates in this energy state.

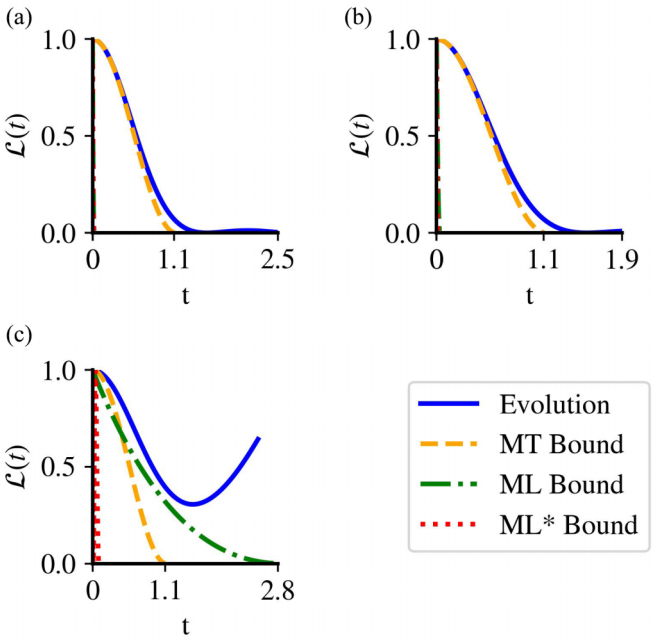

FIG. 3. State evolution of the system for different energy regimes for the Wannier-Stark model, i.e., energy equal to (a) 4900, (b) 3000, and (c) -0.01. Analogously to Fig. 2, we plot the Loschmidt echo from Eq. (4) and from numerical simulation. The initial state is taken to be the eigenstate of the Hamiltonian $H(\Delta_i = 100)$ and this state is quenched by the Hamiltonian $H(\Delta_f = 1.5)$. The system size is $N = 100$.

Next we repeat our argument for the Wannier-Stark model. As expected, the QSL in the Wannier-Stark model shows behavior similar to that of the AA model. The MT bound dominates midspectrum, while the ML bound dominates for low-energy states. Even the crossover is observed in Fig. 3, which was also observed in the case of the AA model.

B. Quench from the delocalized phase to the localized phase

Here we concentrate on the quench from the delocalized phase to the localized phase. First, we consider the AA model. Similar to the results in the preceding section, once again we find that the τ_{QSL} for low- and high-energy states are obeyed by the ML and ML* bounds, respectively, whereas the midspectrum states are MT bounds. As we tend towards the extreme quench regime by increasing Δ_f, the MT bound starts dominating the entire spectrum. Given these results are very similar to those demonstrated in Fig. 1, we do not discuss them explicitly in this section anymore. We choose to analyze in detail how well the bound depicts the exact evolution and the zeros in Loschmidt echo while quenching across the phase boundary. In Fig. 4 we show the results for $\Delta_f > 2$ for the midspectrum states. It can be seen that the MT bound matches with the exact evolution remarkably well until some time and then it starts to deviate from the exact evolution. The

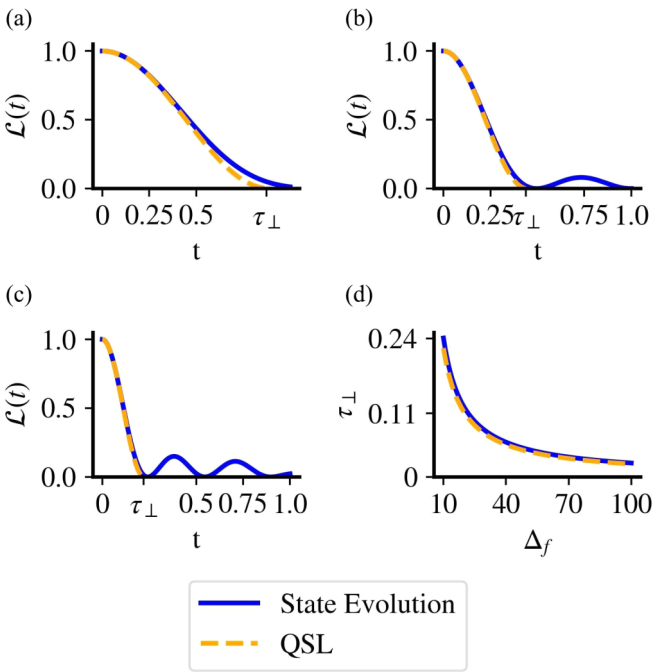

FIG. 4. Comparison of the bound with exact results for an incommensurate lattice. We used Eq. (4) to obtain the Loschmidt echo. The QSL remains consistent with the change in Δ_f: (a) $\Delta_f = 2.5$, (b) $\Delta_f = 5$, and (c) $\Delta_f = 10$. The QSL is the maximum of all three bounds. Here $\Delta_i = 0$ and the system size $N = 100$. (d) The first zero in the Loschmidt echo and the QSL at orthogonal time for different Δ_f values.

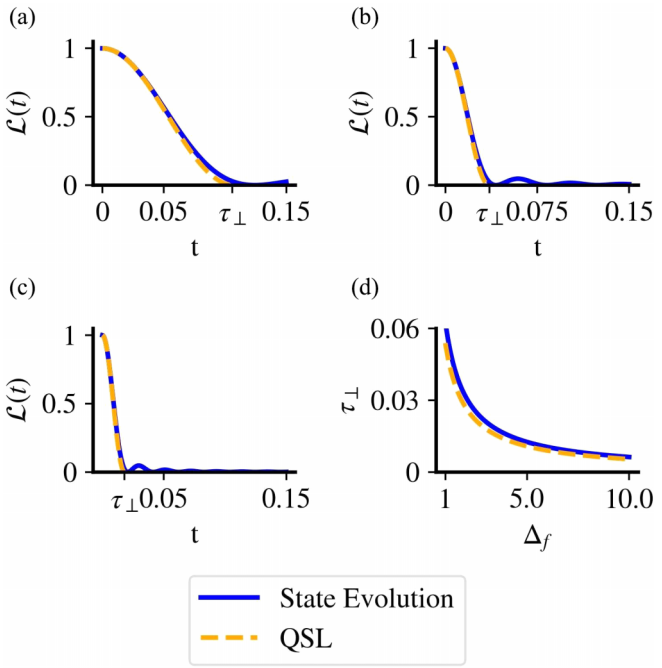

FIG. 5. Comparison of the bound with exact results for the Wannier-Stark model. The QSL bound is compared with the exact dynamics for (a) $\Delta_f = 0.5$, (b) $\Delta_f = 1.5$, and (c) $\Delta_f = 3$, with $\Delta_i = 0$ and system size $N = 100$. (d) First zero in the Loschmidt echo vs Δ_f. We have used Eq. (4) to obtain $\mathcal{L}(t)$.

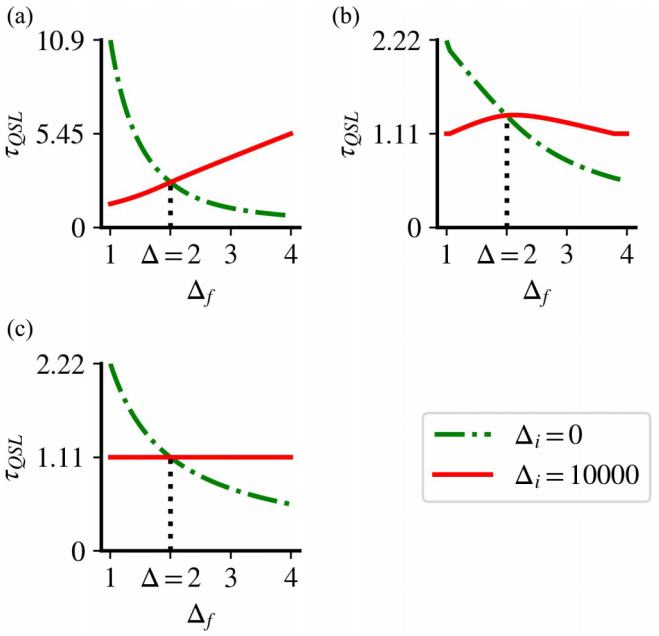

FIG. 6. Plot of τ_{QSL} vs Δ_f for an incommensurate lattice for different energy eigenkets of the Hamiltonian $H(\Delta_i = 0)$: (a) -2.00, (b) -1.41, and (c) 0.00. Here τ_{QSL} is the orthogonalization time of the maximum of all three bounds (4). The system size is taken to be $N = 1000$.

orthogonalization time of the bound is still quite close to the exact orthogonal time $t_\perp$.

Figure 4(d) also shows that the orthogonalization times obtained from both the bound and exact dynamics are inversely proportional to Δ_f. The Wannier-Stark model also shows the same behavior. In the case of the Wannier-Stark model, all states are localized for $\Delta_f > 0$. In Fig. 5 one can see that the Loschmidt echo reaches zero much faster compared to the AA model. Once again, like the AA model, the MT bound matches with the exact evolution remarkably. The orthogonalization time of the bound is reasonably close to the exact orthogonal time, both of which scale as Δ_f^{-1}. This result confirms that indeed the QSL can mimic the exact dynamics of $\mathcal{L}(t)$ reasonably well for both models.

C. Detection of the transition point from the QSL

Here the goal is to identify the transition point using the QSL. Motivated by the analytical results for the extreme quench, we study the variation of τ_{QSL} [see Eq. (1)] with Δ_f. We consider two situations: $\Delta_i = 0$ and $\Delta_i \gg 2$. We find that in a τ_{QSL} vs Δ_f plot for the AA model (Fig. 6), two curves (one corresponding to $\Delta_i = 0$ and the other to $\Delta_i = 10\,000$) intersect at $\Delta_f = 2$ for all initial states. Note that $\Delta = 2$ also corresponds to the localization-delocalization transition point of the AA model. This result does not depend on N as long N is reasonably large.

In contrast to the AA model, for the Wannier-Stark Hamiltonian, in the $N \to \infty$ limit, any infinitesimal Δ is sufficient to localize all eigenstates. However, for finite N, one can have a localization-delocalization phase transition for finite Δ. By following the same procedure as before, we plot in Fig. 7(a) τ_{QSL} vs Δ_f; the two curves (one corresponding to $\Delta_i = 0$ and the other to $\Delta_i = 10\,000$) intersect at $\Delta_f = 0.004\,899$ for $N = 1000$.

This transition point depends on the system size N. In Fig. 7(b) we plot the phase transition point as a function of system size. From the figure it is apparent that as the system size increases, the transition point heads towards zero as N^{-1}. Our finding is consistent with the results obtained from normalized participation ratio calculations as well (see Appendix B).

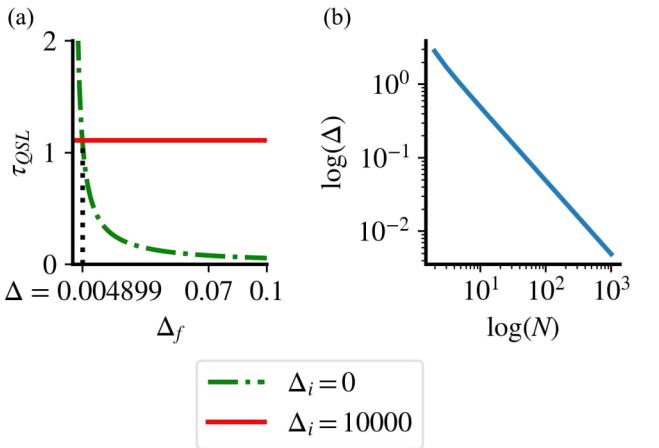

FIG. 7. Transition point for the Wannier-Stark model. (a) Transition point for system size $N = 1000$. (b) A log-log plot of the variation of the transition point with system size N.

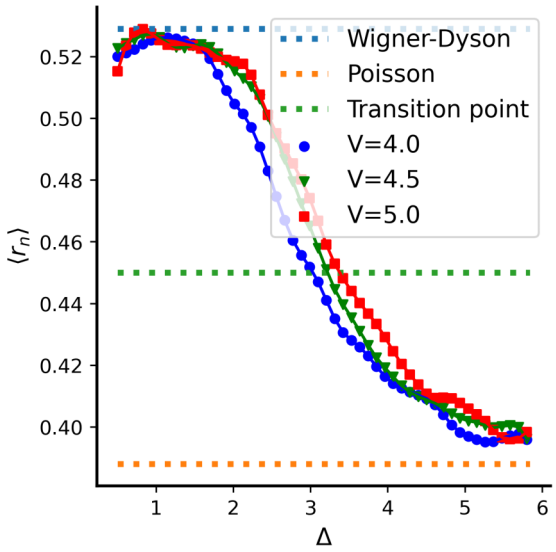

FIG. 8. Plot of average level-spacing characteristics vs on-site potential Δ. Lattice size is taken to be $N = 12$ with half filling.

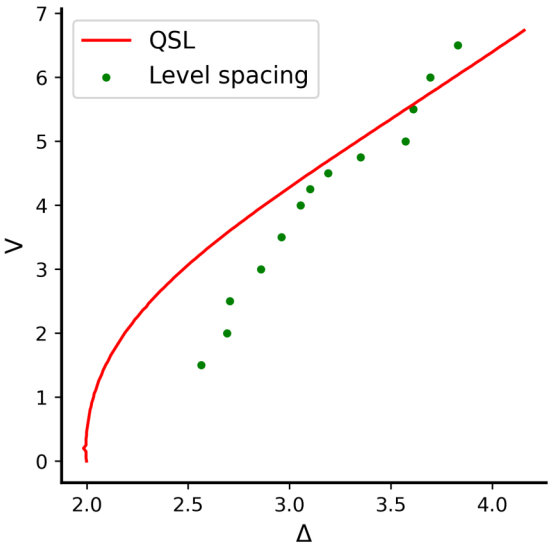

FIG. 9. Detection of many-body localization transitions from the QSL and level-spacing characteristics. We have taken lattice site $N = 12$ with half filling.

D. Detection of the MBL transition point from the QSL

Finally, we consider the interacting system to test our prediction to its full potential. We focus on the Hamiltonian H_{MBL} (3). It is well established that for a fixed interaction strength V, as we increase the strength of the incommensurate potential Δ, the system undergoes an ergodic to many-body localization transition. As we already discussed earlier, in the absence of an interaction, the delocalization-localization transition point corresponds to $\Delta = 2J$, but with the increase of interaction strength, one needs a larger value of Δ to see the transition [49]. Previously, in Sec. IV C, we demonstrated that the QSL can successfully predict the $\Delta = 2J$ transition point for a noninteracting system. Now the question arises whether the QSL can also capture the MBL transition point.

First, we use the level-spacing characteristics to detect the MBL transitions. The level statistics of the many-body Hamiltonian vary from Wigner-Dyson statistics (ergodic phase) to Poissonian statistics (many-body localized phase)[49]. If the energies of the Hamiltonian are written in ascending order $E_1, E_2, \ldots, E_n$, the gap between successive energies is given as $\delta_n = E_{n+1} - E_n$. Then the correlation between successive gaps in the spectrum can be written as

$$r_n = \frac{\min(\delta_n, \delta_{n+1})}{\max(\delta_n, \delta_{n+1})}. \tag{21}$$

We are mainly interested in the average correlation $\langle r_n \rangle$. For Poissonian statistics, we have $\langle r_n \rangle \approx 0.386$, and for Wigner-Dyson statistics, $\langle r_n \rangle \approx 0.5295$. Thus, when we vary Δ in the Hamiltonian H_{MBL} (for a fixed V), we expect the value of the r parameter to decrease from 0.529 (Wigner-Dyson statistics) to 0.386 (Poissonian statistics) with increasing Δ as we approach the ergodic to MBL phase transition. From Fig. 8 we see that for $V = 4, 4.5, 5$, after some critical value of Δ_c, $\langle r_n \rangle$ reaches close to 0.529 and then approaches 0.386 with increasing Δ for $N = 12$. We emphasize, though, that one would expect any tiny amount of Δ to ensure Wigner-Dyson statistics, given the Hamiltonian H_{MBL} is nonintegrable; however, it has been shown that for the finite-size system, one needs a critical value of the integrability breaking parameter to see Wigner-Dyson statistics in level spacing. This critical value of the integrability parameter approaches zero in the thermodynamic limit $N \to \infty$ [52,53]. It has been argued in Ref. [54] that at the MBL transition point, the value of the r parameter is expected to be close to 0.45 for $N = 12$; we use that as a diagnostic tool to identify the transition point for different values of V (see Fig. 8).

Next we focus on finding the MBL transition point from the QSL. First, we take the initial state of the system as the ground state of the prequench Hamiltonian $H_{\mathrm{MBL}}(J = 1, \Delta_i = 0, V)$ and find the QSL as a function of Δ for the postquench Hamiltonian $H_{\mathrm{MBL}}(J = 1, \Delta > 0, V)$. Similarly, we also find the QSL for the initial state, that is, the ground state of the prequench Hamiltonian $H_{\mathrm{MBL}}(J = 1, \Delta_i = 100, V)$, and the postquench Hamiltonian is $H_{\mathrm{MBL}}(J = 1, \Delta < \Delta_i, V)$. As discussed in the previous section, we identify the value of Δ for which these two QSLs will intersect as the transition point for a fixed V. We plot this transition point for different interaction strengths V in Fig. 9. We plot transition points obtained by level-spacing statistics in the same figure. (Note that we have recognized the transition point by identifying Δ for which the value of the r parameter is 0.45 [54]). Remarkably, the transition points obtained from level spacing and the QSL are in great agreement for $V \in [4, 6]$. However, we emphasize that for system size $N \leqslant 16$ (i.e., what is accessible to us using exact diagonalization for the interacting system), if V is reasonably small ($V < 2$) or large ($V > 6.5$), the maximum value of the r parameter remains much smaller than 0.53, which makes our analysis of r parameter to detect the ergodic to MBL transition extremely inefficient for such parameters (see Appendix. D).

V. CONCLUSION

Our main goals were to identify the dynamical regimes of QSL applicability for the many-body physical model and to study the QSL for a many-body system that undergoes phase transitions. To achieve these objectives, we considered the noninteracting Aubry-Andre model, the Wannier-Stark model that shows localization transitions, and the interacting many-body model that shows MBL transitions. We found outstanding agreement between the localization-delocalization transition point obtained using the QSL and the one we found from the normalized participation ratio in the case of the Aubry-Andre and Wannier-Stark Hamiltonians. Furthermore, we also compared the ergodic to MBL transitions found by the QSL and level-spacing characteristics of the many-body interacting Hamiltonian.

In the case of the Aubry-Andre and Wannier-Stark Hamiltonians, we found that for the quench across the phase boundary, the dynamics of the Loschmidt echo can be well described by QSLs. We proved, in the small-time limit, that the MT bound is always tighter compared to the ML and ML* bounds, but for the time of orthogonalization $t_\perp$, the tighter bound can also be a ML or ML* bound, depending on the average energy and energy uncertainty of the initial state. For extreme quenches, i.e., $\Delta \to 0$ to $\Delta \to \infty$ or vice versa, we showed that the MT bound is always tighter for all the states. Moreover, a comparison was made between the time required for the first zero of the Loschmidt echo and the QSL bound corresponding to the time of orthogonalization. While the exact values are a bit different, both of them show qualitatively similar behavior as a function of the quench parameter, e.g., in the case of a quench from the delocalized phase to the localized phase, they scale inversely with Δ, and for the opposite quench, they remain independent of Δ. Most strikingly, we found that if the prequench Hamiltonian is either deep inside the delocalized phase or deep into the localized phase, for both cases, the τ_{QSL} remains the same if the postquench Hamiltonian corresponds to the Hamiltonian at the transition point. This fact can be used as a diagnostic tool to detect the transition point. Moreover, we also used the same QSL protocol for interacting systems that show the ergodic to MBL transition. First, we used the level-spacing statistic to identify the transition point and then compared it with the one obtained using the QSL protocol to find very good agreement for a certain parameter regime.

The time development of the mean return probability of the projectors provides a universal bound [55,56] for the spectral form factor [57–59] through which the minimum time required for certain versions of scrambling can be detected. Also, universal results on the minimum time required for the scrambling, and thereby the time at which the application of the equilibrium thermodynamics is studied, were obtained. The dependence of the QSL on the initial state was averaged by considering mean return probability, a function of the QSL. Our work complements these studies, in which we studied localization transitions, and even though the QSL depends on the initial state, the quenching from two extreme states (completely localized and completely delocalized states) provides a kind of averaging and the QSL captures the transition and dynamics effectively. We expect that the QSL will play an important part in further understanding the many-body theory and phase transitions. In particular, it would be interesting to study the role of the universal bound proposed in Refs. [55,56] in future studies.

While there exist a large number of tools to detect localization-delocalization transition points such as participation ratio [60,61], entanglement entropy [62], energy spacing statistics [60], and observational entropy [63], computation-wise τ_{QSL} is much simpler compared to any of them. It does not involve diagonalization of the entire Hamiltonian, nor does one need to compute the exact dynamics; one simply needs to calculate the energy expectation and the energy variance. Given the Hamiltonian of interest is usually a sparse matrix, such operations are much less cumbersome. We believe that, especially in the case of the many-body Hamiltonian, to detect the ergodic to many-body localization transition, our diagnostic tool should be a great advantage over the existing ones.

ACKNOWLEDGMENTS

R.M. acknowledges the DST-Inspire fellowship by the Department of Science and Technology, Government of India, SERB start-up grant (Grant No. SRG/2021/002152). S.A. acknowledges the start-up research grant from SERB, Department of Science and Technology, Government of India (Grant No. SRG/2022/000467).

APPENDIX A: DETAILS OF THE CALCULATION OF $\langle H^2(\Delta_f = 0)\rangle$

In this Appendix we discuss the details of the calculation of $\langle H\rangle$ and $\langle H^2\rangle$ for extreme quench, i.e., $\Delta_i \to \infty$ to $\Delta_f \to 0$. At $\Delta_f = 0$ the diagonal entries of the Hamiltonian are zero. Thus, the Hamiltonian and square of the Hamiltonian take the form

$$H = -J\sum_{k=1}^{N}(c_{k+1}^\dagger c_k + c_k^\dagger c_{k+1}),$$

$$H^2 = J^2\sum_{k=1}^{N}\sum_{l=1}^{N}(c_{k+1}^\dagger c_k + c_k^\dagger c_{k+1})(c_{l+1}^\dagger c_l + c_l^\dagger c_{l+1}),$$

$$H^2 = J^2\sum_{k=1}^{N}\sum_{l=1}^{N}(c_{k+1}^\dagger c_k c_{l+1}^\dagger c_l + c_k^\dagger c_{k+1}c_{l+1}^\dagger c_l + c_{k+1}^\dagger c_k c_l^\dagger c_{l+1} + c_k^\dagger c_{k+1}c_l^\dagger c_{l+1}).$$

As the initial state is taken as one of the eigenstates of the Hamiltonian $H(\Delta_i \to \infty)$, the eigenstates have the form $|\psi\rangle = c_m^\dagger|0\rangle$, $m = 1, 2, \ldots, N$. The expectation value of the Hamiltonian with respect to the above initial states can be computed as

$$\langle H\rangle = \sum_{k=1}^{N}[\langle 0|c_m c_{k+1}^\dagger c_k c_m^\dagger|0\rangle + \langle 0|c_m c_k^\dagger c_{k+1}c_m^\dagger|0\rangle],$$

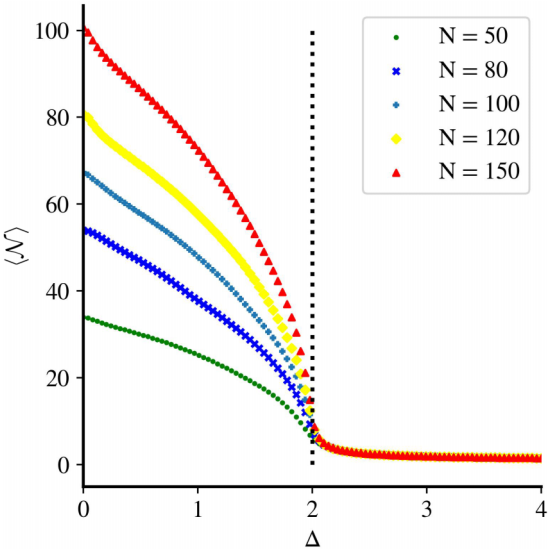

FIG. 10. Average normalized participation ratio vs Δ for the incommensurate model. The dotted line indicates the phase transition calculated from the QSL.

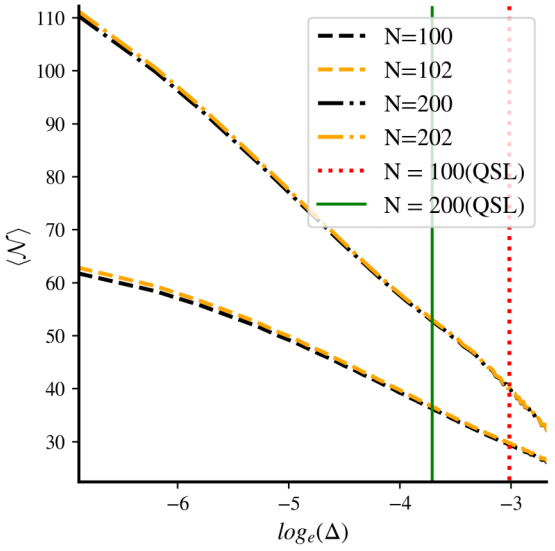

FIG. 11. Average normalized participation ratio vs Δ for the Wannier-Stark model. The vertical line indicates the phase transition calculated from the QSL.

$$\langle H \rangle = 0.$$

Similarly, the average of the square can be written as

$$\begin{aligned}\langle H^2 \rangle = J^2 \sum_{k=1}^{N}\sum_{l=1}^{N}[&\langle 0|c_m c_{k+1}^\dagger c_k c_{l+1}^\dagger c_l c_m^\dagger|0\rangle \\ &+ \langle 0|c_m c_k^\dagger c_{k+1} c_{l+1}^\dagger c_l c_m^\dagger|0\rangle \\ &+ \langle 0|c_m c_{k+1}^\dagger c_k c_l^\dagger c_{l+1} c_m^\dagger|0\rangle \\ &+ \langle 0|c_m c_k^\dagger c_{k+1} c_l^\dagger c_{l+1} c_m^\dagger|0\rangle].\end{aligned} \tag{A1}$$

For an initial state where $m \neq 1$ or $m \neq N$, the first term and last term go to zero and the other term equals one. Hence $\langle H^2 \rangle = 2J^2$. For the initial state where $m = 1$ or $m = N$, the third or fourth term and the first and second terms go to zero. Hence, for such a state, $\langle H^2 \rangle = J^2$.

APPENDIX B: PARTICIPATION RATIO CALCULATIONS TO DETECT THE TRANSITION POINT

In this Appendix we use the participation ratio as another diagnostic tool to detect the localization-delocalization transition point. The normalized participation ratio (NPR) $\mathcal{N}$ [64] of an eigenstate $|\psi_k\rangle$ of the Hamiltonian $H(\Delta)$ (we set $J = 1$) is given by

$$\mathcal{N}_k = \frac{1}{N\sum_{n=1}^{N}|\langle n|\psi_k\rangle|^4}.$$

Here $|n\rangle = c_n^\dagger|0\rangle$ stands for the Fock space basis for the lattice. If states are completely localized on a given site then $\mathcal{N} = 1/N$. If states are completely delocalized then $\mathcal{N} = N$. Here we calculate the average NPR by taking an average over all the eigenstates of the Hamiltonian $H(\Delta)$.

In the case of the AA model, from Fig. 10 it is clear that there is a phase transition point at $\Delta = 2$. In the region $\Delta < 2$, all the states are delocalized (the mean NPR increases with N), and for $\Delta > 2$, all the states are localized (the mean NPR is independent of N).

For the finite-size Wannier-Stark model, it is known that the transition point varies with system size. However, finding such an N-dependent transition point is quite nontrivial. In the case of the AA model, such an issue does not arise. Hence, we could plot the NPR for different values of N, and if N is sufficiently large, we could easily distinguish the delocalized and localized phases. In the case of the Wannier-Stark model, we expect that if we plot $\mathcal{N}$ for two system sizes N and $N + \Delta N$ (where ΔN is small) beyond a certain Δ_c, the NPR data will almost become indistinguishable, which can be identified as the transition point for system size N. To see this, we plot $\langle \mathcal{N} \rangle$ for two systems whose system size differences are very small. In Fig. 11 we consider system sizes of 100 and 102; the point from which the $\langle \mathcal{N} \rangle$ of both systems start overlapping will be the transition point. We also plot the same for system sizes 200 and 202. From the plot it is clear that the transition point tends to decrease with increasing system size. The vertical lines in the figure, which represent the QSL, also predict the same. Furthermore, the QSL prediction of the transition points is approximately equal to those points from which the data of the NPR start overlapping. For $N \to \infty$, the NPR data will start overlapping even from an infinitesimal value of Δ, and so will the transition point obtained from the QSL, implying any tiny value of the potential Δ is enough to localize all the eigenstates.

APPENDIX C: FINITE-SIZE DEPENDENCE ON THE QSL OF THE AA MODEL

For the thermodynamic limit, in Eqs. (12) and (13) we have approximated averages of cos and $\cos^2$ as 0 and 1/2, respectively. However, for a finite value of N, we can calculate

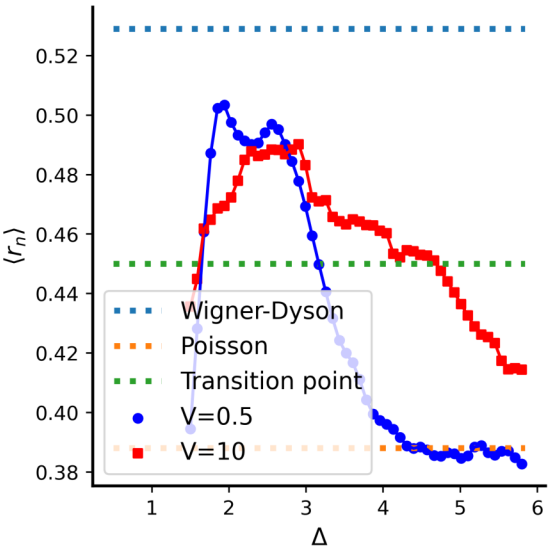

FIG. 12. Plot of average level-spacing statistics vs Δ for different values of the interaction potential V. The system size is taken to be $L = 12$ with half filling

the exact summation as

$$\sum_{n=1}^{N} \cos(2\pi\alpha n) = \sum_{n=1}^{N} \left(\frac{e^{2i\pi\alpha n} + e^{-2i\pi\alpha n}}{2} \right). \tag{C1}$$

From geometric series, it can be proved that

$$\sum_{n=1}^{N} x^n = \frac{x(1-x^n)}{1-x}. \tag{C2}$$

Using this, Eq. (C1) can be simplified to

$$g(N,\alpha) \equiv \sum_{n=1}^{N} \cos(2\pi\alpha n) = \frac{\cos(2\pi\alpha) - \cos[2\pi\alpha(N+1)] + \cos(2\pi\alpha N) - 1}{2[1-\cos(2\pi\alpha)]}. \tag{C3}$$

Similarly, it is easier to obtain

$$\sum_{n=1}^{N} \cos^2(2\pi\alpha n) = \frac{N}{2} + g(N, 2\alpha). \tag{C4}$$

Thus, the uncertainty reads [referring to Eqs. (12) and (13)]

$$\Delta H = \Delta_f \sqrt{\left(\frac{1}{2} + \frac{1}{N} g(N, 2\alpha) - \frac{1}{N^2} g^2(N,\alpha) \right)}. \tag{C5}$$

Thus, at the thermodynamic limit, the leading-order term of $(\Delta H)^2$ for the AA model is $\Delta_f^2/2$. In the case of the Wannier-Stark model, we observed that the leading order of $(\Delta H)^2$ itself was proportional to $\Delta_f^2(N^2-1)$, with a missing higher-order term.

APPENDIX D: LEVEL-SPACING STATISTICS FOR $V = 0.5$ AND 10

As we discussed in Sec. IV D, for small V and large V, the maximum value of the r parameter remains much smaller than 0.529. This is illustrated in Fig. 12. This makes our level-spacing analysis inefficient in detecting the transition point.

[1] J. Anandan and Y. Aharonov, Geometry of quantum evolution, Phys. Rev. Lett. **65**, 1697 (1990).

[2] L. Mandelstam and I. Tamm, The Uncertainty Relation Between Energy and Time in Non-relativistic Quantum Mechanics, in *Selected Papers* edited by B. M. Bolotovskii, V. Y. Frenkel, and R. Peierls (Springer, Berlin, Heidelberg, 1991), pp. 115–123.

[3] M. Okuyama and M. Ohzeki, Quantum speed limit is not quantum, Phys. Rev. Lett. **120**, 070402 (2018).

[4] B. Shanahan, A. Chenu, N. Margolus, and A. del Campo, Quantum speed limits across the quantum-to-classical transition, Phys. Rev. Lett. **120**, 070401 (2018).

[5] K. Kobayashi and N. Yamamoto, Quantum speed limit for robust state characterization and engineering, Phys. Rev. A **102**, 042606 (2020).

[6] T. Hatomura, Performance evaluation of invariant-based inverse engineering by quantum speed limits, Phys. Rev. A **106**, L040401 (2022).

[7] J. M. Epstein and K. B. Whaley, Quantum speed limits for quantum-information-processing tasks, Phys. Rev. A **95**, 042314 (2017).

[8] T. Caneva, M. Murphy, T. Calarco, R. Fazio, S. Montangero, V. Giovannetti, and G. E. Santoro, Optimal control at the quantum speed limit, Phys. Rev. Lett. **103**, 240501 (2009).

[9] S. Lloyd, Computational capacity of the universe, Phys. Rev. Lett. **88**, 237901 (2002).

[10] Y. Maleki, B. Ahansaz, and A. Maleki, Speed limit of quantum metrology, Sci. Rep. **13**, 12031 (2023).

[11] D. P. Pires, M. Cianciaruso, L. C. Céleri, G. Adesso, and D. O. Soares-Pinto, Generalized geometric quantum speed limits, Phys. Rev. X **6**, 021031 (2016).

[12] A. Chenu, M. Beau, J. Cao, and A. del Campo, Quantum simulation of generic many-body open system dynamics using classical noise, Phys. Rev. Lett. **118**, 140403 (2017).

[13] A. D. Cimmarusti, Z. Yan, B. D. Patterson, L. P. Corcos, L. A. Orozco, and S. Deffner, Environment-assisted speed-up of the field evolution in cavity quantum electrodynamics, Phys. Rev. Lett. **114**, 233602 (2015).

[14] X.-M. Zhang, Z.-W. Cui, X. Wang, and M.-H. Yung, Automatic spin-chain learning to explore the quantum speed limit, Phys. Rev. A **97**, 052333 (2018).

[15] N. Margolus and L. B. Levitin, The maximum speed of dynamical evolution, Physica D **120**, 188 (1998).

[16] G. Ness, A. Alberti, and Y. Sagi, Quantum speed limit for states with a bounded energy spectrum, Phys. Rev. Lett. **129**, 140403 (2022).

[17] L. B. Levitin and T. Toffoli, Fundamental limit on the rate of quantum dynamics: The unified bound is tight, Phys. Rev. Lett. **103**, 160502 (2009).

[18] M. E. Fisher, *The Nature of Critical Points*, Lectures in Theoretical Physics Vol. VII (University of Colorado Press, Boulder, 1965).

[19] G. Mussardo, *Statistical Field Theory: An Introduction to Exactly Solved Models in Statistical Physics* (Oxford University Press, New York, 2010).

[20] M. Heyl, A. Polkovnikov, and S. Kehrein, Dynamical quantum phase transitions in the transverse-field Ising model, Phys. Rev. Lett. **110**, 135704 (2013).

[21] C. Karrasch and D. Schuricht, Dynamical phase transitions after quenches in nonintegrable models, Phys. Rev. B **87**, 195104 (2013).

[22] J. M. Hickey, S. Genway, and J. P. Garrahan, Dynamical phase transitions, time-integrated observables, and geometry of states, Phys. Rev. B **89**, 054301 (2014).

[23] E. Canovi, P. Werner, and M. Eckstein, First-order dynamical phase transitions, Phys. Rev. Lett. **113**, 265702 (2014).

[24] F. Andraschko and J. Sirker, Dynamical quantum phase transitions and the Loschmidt echo: A transfer matrix approach, Phys. Rev. B **89**, 125120 (2014).

[25] M. Heyl, Quenching a quantum critical state by the order parameter: Dynamical quantum phase transitions and quantum speed limits, Phys. Rev. B **95**, 060504(R) (2017).

[26] M. Heyl, Dynamical quantum phase transitions: A review, Rep. Prog. Phys. **81**, 054001 (2018).

[27] Y. Zeng, B. Zhou, and S. Chen, Dynamical singularity of the rate function for quench dynamics in finite-size quantum systems, Phys. Rev. B **107**, 134302 (2023).

[28] B. Zhou, Y. Zeng, and S. Chen, Exact zeros of the Loschmidt echo and quantum speed limit time for the dynamical quantum phase transition in finite-size systems, Phys. Rev. B **104**, 094311 (2021).

[29] S. Vajna and B. Dóra, Topological classification of dynamical phase transitions, Phys. Rev. B **91**, 155127 (2015).

[30] U. Bhattacharya and A. Dutta, Emergent topology and dynamical quantum phase transitions in two-dimensional closed quantum systems, Phys. Rev. B **96**, 014302 (2017).

[31] R. Jafari, A. Akbari, U. Mishra, and H. Johannesson, Floquet dynamical quantum phase transitions under synchronized periodic driving, Phys. Rev. B **105**, 094311 (2022).

[32] S. Zamani, R. Jafari, and A. Langari, Out-of-time-order correlations and Floquet dynamical quantum phase transition, Phys. Rev. B **105**, 094304 (2022).

[33] P. Jurcevic, H. Shen, P. Hauke, C. Maier, T. Brydges, C. Hempel, B. P. Lanyon, M. Heyl, R. Blatt, and C. F. Roos, Direct observation of dynamical quantum phase transitions in an interacting many-body system, Phys. Rev. Lett. **119**, 080501 (2017).

[34] S. Smale, P. He, B. A. Olsen, K. G. Jackson, H. Sharum, S. Trotzky, J. Marino, A. M. Rey, and J. H. Thywissen, Observation of a transition between dynamical phases in a quantum degenerate Fermi gas, Sci. Adv. **5**, eaax1568 (2019).

[35] C. Yang, Y. Wang, P. Wang, X. Gao, and S. Chen, Dynamical signature of localization-delocalization transition in a one-dimensional incommensurate lattice, Phys. Rev. B **95**, 184201 (2017).

[36] R. Modak and D. Rakshit, Many-body dynamical phase transition in a quasiperiodic potential, Phys. Rev. B **103**, 224310 (2021).

[37] M. Faridfar, A. A. Fouladi, and J. Vahedi, Dynamical quantum phase transitions in stark quantum spin chains, Physica A **619**, 128732 (2023).

[38] S. Aubry and G. André, Analyticity breaking and Anderson localization in incommensurate lattices, in *Proceedings, VIII International Colloquium on Group-Theoretical Methods in Physics* (1980), Vol. 3.

[39] D. Emin and C. F. Hart, Existence of Wannier-Stark localization, Phys. Rev. B **36**, 7353 (1987).

[40] G. H. Wannier, Dynamics of band electrons in electric and magnetic fields, Rev. Mod. Phys. **34**, 645 (1962).

[41] D. A. Abanin, E. Altman, I. Bloch, and M. Serbyn, *Colloquium*: Many-body localization, thermalization, and entanglement, Rev. Mod. Phys. **91**, 021001 (2019).

[42] J. Billy, V. Josse, Z. Zuo, A. Bernard, B. Hambrecht, P. Lugan, D. Clément, L. Sanchez-Palencia, P. Bouyer, and A. Aspect, Direct observation of Anderson localization of matter waves in a controlled disorder, Nature (London) **453**, 891 (2008).

[43] F. Jendrzejewski, A. Bernard, K. Mueller, P. Cheinet, V. Josse, M. Piraud, L. Pezzé, L. Sanchez-Palencia, A. Aspect, and P. Bouyer, Three-dimensional localization of ultracold atoms in an optical disordered potential, Nat. Phys. **8**, 398 (2012).

[44] S. S. Kondov, W. R. McGehee, J. J. Zirbel, and B. DeMarco, Three-dimensional Anderson localization of ultracold matter, Science **334**, 66 (2011).

[45] S. R. Taylor, M. Schulz, F. Pollmann, and R. Moessner, Experimental probes of Stark many-body localization, Phys. Rev. B **102**, 054206 (2020).

[46] E. E. Mendez, F. Agulló-Rueda, and J. M. Hong, Stark localization in GaAs-GaAlAs superlattices under an electric field, Phys. Rev. Lett. **60**, 2426 (1988).

[47] G. Roati, C. D'Errico, L. Fallani, M. Fattori, C. Fort, M. Zaccanti, G. Modugno, M. Modugno, and M. Inguscio, Anderson localization of a non-interacting Bose–Einstein condensate, Nature (London) **453**, 895 (2008).

[48] M. Schreiber, S. S. Hodgman, P. Bordia, H. P. Lüschen, M. H. Fischer, R. Vosk, E. Altman, U. Schneider, and I. Bloch, Observation of many-body localization of interacting fermions in a quasirandom optical lattice, Science **349**, 842 (2015).

[49] S. Iyer, V. Oganesyan, G. Refael, and D. A. Huse, Many-body localization in a quasiperiodic system, Phys. Rev. B **87**, 134202 (2013).

[50] L. D. Faddeev, in *Fifty Years of Mathematical Physics*, edited by M. Ge and A. J. Niemi (World Scientific, Singapore, 2016), Vol. 2, pp. 370–439.

[51] R. Bhatia and C. Davis, A better bound on the variance, Amer. Math. Monthly **107**, 353 (2000).

[52] R. Modak, S. Mukerjee, and S. Ramaswamy, Universal power law in crossover from integrability to quantum chaos, Phys. Rev. B **90**, 075152 (2014).

[53] R. Modak and S. Mukerjee, Finite size scaling in crossover among different random matrix ensembles in microscopic lattice models, New J. Phys. **16**, 093016 (2014).

[54] P. Sierant and J. Zakrzewski, Level statistics across the many-body localization transition, Phys. Rev. B **99**, 104205 (2019).

[55] A. Vikram and V. Galitski, Exact universal bounds on quantum dynamics and fast scrambling, Phys. Rev. Lett. **132**, 040402 (2024).

[56] A. Vikram, L. Shou, and V. Galitski, Proof of a universal speed limit on fast scrambling in quantum systems, arXiv:2404.15403.

[57] F. Haake, *Quantum Signatures of Chaos* (Springer, 1991).

[58] S. Müller, S. Heusler, P. Braun, F. Haake, and A. Altland, Semiclassical foundation of universality in quantum chaos, Phys. Rev. Lett. **93**, 014103 (2004).

[59] A. Vikram and V. Galitski, Dynamical quantum ergodicity from energy level statistics, Phys. Rev. Res. **5**, 033126 (2023).

[60] P. Chatterjee and R. Modak, One-dimensional Lévy quasicrystal, J. Phys.: Condens. Matter **35**, 505602 (2023).

[61] R. Modak, S. Mukerjee, E. A. Yuzbashyan, and B. S. Shastry, Integrals of motion for one-dimensional Anderson localized systems, New J. Phys. **18**, 033010 (2016).

[62] R. Modak, S. Ghosh, and S. Mukerjee, Criterion for the occurrence of many-body localization in the presence of a single-particle mobility edge, Phys. Rev. B **97**, 104204 (2018).

[63] R. Modak and S. Aravinda, Observational-entropic study of Anderson localization, Phys. Rev. A **106**, 062217 (2022).

[64] S. Roy, S. Chattopadhyay, T. Mishra, and S. Basu, Critical analysis of the reentrant localization transition in a one-dimensional dimerized quasiperiodic lattice, Phys. Rev. B **105**, 214203 (2022).